Available online at www.sciencedirect.com

ScienceDirect

Advances in Space Research xxx (xxxx) xxx

ADVANCES IN SPACE RESEARCH (a COSPAR publication)

www.elsevier.com/locate/asr

Stochastic optimization for stationkeeping of periodic orbits using a high-order Target Point Approach

Xiaoyu Fu [a,*], Nicola Baresi [a], Roberto Armellin [b]

[a] Surrey Space Centre, University of Surrey, GU2 7XH Guildford, United Kingdom
[b] Te Pūnaha Ātea - Auckland Space Institute, University of Auckland, Auckland, New Zealand

Received 27 February 2022; received in revised form 9 April 2022; accepted 15 April 2022

Abstract

Periodic orbits in the Restricted Three-Body Problem are widely adopted as nominal trajectories by different missions. To maintain periodic orbits in a three-body regime, a stationkeeping strategy based on a high-order Target Point Approach (TPA) is proposed, where fuel-optimal and error-robust TPA parameters are acquired from stochastic global optimization. Accurate TPA maneuvers are calculated in a high-order fashion enabled by Differential Algebra techniques. Orbit determination epoch is selected using a sensitivity analysis based on the convergence radius of a stroboscopic map. Stochasticity is handled by incorporating Monte Carlo simulations in the process of optimization and the evaluation of high-order ODE expansions is employed to supplant the time-consuming numerical integration. Two specific types of periodic orbits, Near Rectilinear Halo Orbits and Quasi-Satellite Orbits, are investigated to demonstrate the validity and efficiency of the strategy.

Keywords: Stochastic optimization; Periodic orbits; Stationkeeping; Differential Algebra; Target Point Approach

1. Introduction

Research enthusiasm on periodic orbits in the Restricted Three-Body Problem never wanes. Different types of periodic orbits with favorable properties are widely adopted in various space missions. As orbits generated in a three-body regime, periodic orbits are sensitive to perturbations and thereby, a stationkeeping scheme is essential for the long-term orbital maintenance of periodic orbits in a chaotic dynamical environment.

Various stationkeeping techniques concerning the control of different periodic orbits have been investigated in previous research. The Floquet mode control (Howell and Keeter, 1995; Gómez et al., 1998) was developed to cancel the unstable mode for a reference orbit and adopted for the maintenance of multiple linearly unstable Halo orbits. Another stationkeeping method tailed for periodic orbits is the Hamiltonian-structure preserving control (Scheeres et al., 2003; Xu and Xu, 2009b), in which a feedback control law is specified by the instantaneous eigenstructure of an unstable periodic orbit. The Cauchy-Green Tensor approach and x-axis crossing control strategy were thoroughly investigated for the stationkeeping problems in the Earth-Moon system by Guzzetti et al. (2017). Methods developed from classical control theories, including nonlinear programming (Ghorbani and Assadian, 2013), pole assignment technique (Gurfil and Meltzer, 2006), and H_∞ control (Kulkarni et al., 2006), were applied to the stationkeeping problem in multi-body regimes. A detailed categorization and elaboration of the stationkeeping methods for libration point orbits was provided by Shirobokov et al. (2017).

* Corresponding author.
E-mail addresses: x.fu@surrey.ac.uk (X. Fu), n.baresi@surrey.ac.uk (N. Baresi), roberto.armellin@auckland.ac.nz (R. Armellin).

https://doi.org/10.1016/j.asr.2022.04.039
0273-1177/

Among the existing techniques, the Target Point Approach (TPA) was initially introduced to compute correction maneuvers by minimizing a weighted cost function which is defined in terms of maneuvers and position and velocity deviations from a nominal trajectory at specified locations (Howell and Pernicka, 1993). Multiple targeting strategies were derived from the TPA and widely adopted in different mission scenarios (Gómez et al., 1998; Oguri et al., 2020; Dei Tos et al., 2020). However, there still exist major limitations in the stationkeeping strategies based on TPA.

Firstly, since the analytical corrective maneuvers of TPA are deduced linearly by means of state transition matrices, a resulting omission of high-order information could possibly lead to inaccurate maneuvers, which would augment the deviation in trajectory propagation. Furthermore, the accumulating inaccuracy would even lead to a higher propellant cost in the long term. Such a situation could even worsen when dealing with unstable periodic orbits which require more frequent maneuvers for an effective orbit maintenance (Muralidharan and Howell, 2020).

Secondly, TPA depends on various parameters which dominate its long-term stationkeeping cost and the boundedness of a controlled trajectory. At the initial phase of TPA research, most TPA parameters are acquired through trial and error due to a limited computational capacity (Howell and Pernicka, 1993). Subsequently, global optimization techniques are applied to acquire the optimal TPA parameters in a unified approach by Dei Tos and Baresi (2020). In their work, reasonable simplifications have been made to reduce the search space of optimization and promising results have been achieved. However, there is still a relative lack of knowledge about the relation between the optimal TPA parameters and the periodicity of a candidate periodic orbit. In addition, due to the existence of time-consuming numerical integration in fitness evaluation, a compromise on the number of Monte Carlo (MC) samples has to be forged in their optimization, which to some extent undermines the optimality of the acquired TPA parameters.

The reality is that errors from different sources, including navigation uncertainty, control noise, and dynamics inaccuracy can render a stationkeeping strategy infeasible. Consequently, it is crucial to develop an effective method to handle the stochasticity in the determination of optimal stationkeeping parameters. Multiple stochastic optimization techniques are developed in previous research to tackle uncertainty in different spacecraft trajectory design problems. A sequential optimization and reliability assessment process is proposed to realize a soft landing in an uncertain asteroid environment (Ren and Shan, 2015). Unscented guidance is introduced by combining the concept of unscented transform with standard optimal control, and applied to orbital and proximity operations in an uncertain environment (Ross et al., 2014). A multi-objective uncertainty optimization with a weighted energy-covariance cost function is developed and tested in three maneuver scenarios related with an uncertain asteroids environment (Jenson and Scheeres, 2021a).

In comparison, the application of stochastic optimization in station-keeping astrodynamics problems is quite limited and often reduced to a posteriori MC analyses. By incorporating MC simulations in the optimization of stationkeeping parameters, optimal error-robust stationkeeping strategy can be achieved. Unfortunately, this seemingly approachable solution is fairly challenging, since the number of MC samples has to be sufficiently large to guarantee the statistical significance of optimization results. Such an analysis usually comes at the cost of a higher computational effort, due to the large number of ODE integration required in a reliable station-keeping simulation.

In this research, we propose a nonlinear station-keeping strategy for periodic orbits, in which accurate TPA maneuvers are calculated with a high-order maneuver map enabled by Differential Algebra (DA) techniques. The DA framework (Berz, 1999) was originally developed and applied in the field of particle accelerator physics. Inspired by its success, astrodynamics researchers have later found fertile ground for DA-based applications in a variety of orbital mechanics and uncertainty propagation problems (Armellin et al., 2010a; Morselli et al., 2014; Armellin et al., 2015; Wittig et al., 2015). Critical DA techniques leveraged in this work are the high-order expansion of an ODE flow and the partial inversion of a polynomial map. By combining these two methods, a stochastic optimization framework for station-keeping applications can be developed whereby fuel-optimal and error-robust TPA parameters can be generated via pre-computed flow maps that efficiently replace numerically expensive ODE integrations. It needs to be remarked that in this research, an expansion order of 6 is employed for all the DA operations. Such a choice of expansion order is found to provide a suitable compromise between the accuracy of a Taylor expansion and the computation time in most Astrodynamics applications (Armellin et al., 2010a; Wittig et al., 2015).

This paper is organized as follows. We start by reviewing the background knowledge of the Circular Restricted Three-body Problem (CRTBP), periodic orbits, and linear TPA approach. In the subsequent "Methodology" section, the high-order TPA method is first introduced and later analyzed within the context of a TPA-based stationkeeping strategy for periodic orbits. With these two theoretical foundations, a stochastic optimization framework in search of error-robust TPA parameters is elaborated. Stationkeeping analyses of Near Rectilinear Halo Orbits (NRHOs) and Quasi-Satellite Orbits (QSOs) are executed to corroborate the effectiveness of the proposed methodology and evaluate the performance of the proposed approach. Conclusions are drawn in the final section of this paper.

2. Technical background

In this section, the equations of the CRTBP and two specific types of periodic orbits, NRHOs and QSOs, are first presented. The linear TPA is introduced subsequently to support the mathematical developments required for the proposed high-order TPA method.

2.1. Circular restricted three-body problem

In the CRTBP, the motion of a mass particle m is governed by the gravitational fields of two spherical bodies, m_1 and m_2, which are in a circular orbit around each other. Typically, the motion of the particle is investigated in a rotating coordinate frame, where the barycenter of the two bodies, i.e. the primaries, is taken as the origin of the system, whereas the x-axis is chosen such that the two primaries keep stationary along this axis. In addition, normalized units are selected and utilized in the coordinates: the unit of length is chosen to match the constant distance between the two masses; the unit of mass is chosen to be the sum of the primaries' mass; the unit of time is chosen such that the orbital period of the primaries about their barycenter is equal to 2π. By means of the normalization above, the only parameter of the system remains the mass ratio parameter, μ, which is given by

$$\mu = \frac{m_2}{m_1 + m_2}.$$

The equation of motion (EOM) of CRTBP in the rotating coordinate frame are then:

$$\ddot{x} - 2\dot{y} = -\overline{U}_x \tag{1}$$

$$\ddot{y} - 2\dot{x} = -\overline{U}_y \tag{2}$$

$$\ddot{z} = -\overline{U}_z \tag{3}$$

where (x, y, z) and $(\dot{x}, \dot{y}, \dot{z})$ denote the position and velocity components of a particle in the rotating frame. $\overline{U}$ corresponds to the effective potential and is defined as

$$\overline{U} = -\frac{1}{2}(x^2 + y^2) - \frac{\mu_1}{r_1} - \frac{\mu_2}{r_2} - \frac{1}{2}\mu_1\mu_2 \tag{4}$$

The subscripts of $\overline{U}$ in the EOM denote its corresponding partial derivatives. r_1 and r_2 denote the distances from the particle to the primaries, whereas $\mu_1 = (1 - \mu)$ and $\mu_2 = \mu$ represent the normalized masses of the two primaries.

It can be proved that the CRTBP is a Hamiltonian time-invariant system with one integral of motion known as the Jacobi constant:

$$C(x, y, z, \dot{x}, \dot{y}, \dot{z}) = -\left(\dot{x}^2 + \dot{y}^2 + \dot{z}^2\right) - 2\overline{U}(x, y, z) \tag{5}$$

2.2. Periodic orbits in CRTBP

Since the Jacobi Constant is the only integral of motion of the CRTBP, Eq. (1) cannot be solved in closed-form and is non-integrable. Following Poincaré's theories, special-case solutions such as equilibrium points and periodic orbits were then discovered and investigated to comprehend the dynamical features of CRTBP. Two specific types of periodic orbits, NRHOs and QSOs, are hereby taken into account and further investigated as the test cases in this stationkeeping analysis.

2.2.1. Near rectilinear halo orbits

NRHOs have witnessed an increasing research interest due to their advantages in linear stability characteristics, close lunar passages, and nearly uninterrupted lunar communication links (Guzzetti et al., 2017; Davis et al., 2017). Standing as the candidate orbits for the Lunar Orbital Platform-Gateway (LOP-G) mission, NRHOs will function as a staging post in the cislunar region for both lunar missions and deep space explorations (Crusan et al., 2018). As a subset of the Halo orbit family around the L_1 and L_2 libration points in the CRTBP, NRHOs are three-dimensional orbits with close proximity to the secondary body. As a demonstration, the southern Halo orbit family in the vicinity of L_2 in the Earth-Moon system is shown in Fig. 1, with its NRHO members highlighted in light blue.

To further establish the boundaries of the NRHO portion in a Halo family, the following stability indices v_i are defined:

$$v_i = \frac{1}{2}\left(\lambda_i + \frac{1}{\lambda_i}\right), \text{for} i = 1, 2 \tag{6}$$

where λ_i and $\frac{1}{\lambda_i}$ comprise the reciprocal pair of eigenvalues of a monodromy matrix, i.e. the state transition matrix (STM) integrated over one revolution. If both stability indices, v_1 and v_2, are no larger than one in modulus, then the corresponding orbit is linearly stable; otherwise, the orbit is unstable, in a linear sense. The larger the magnitude

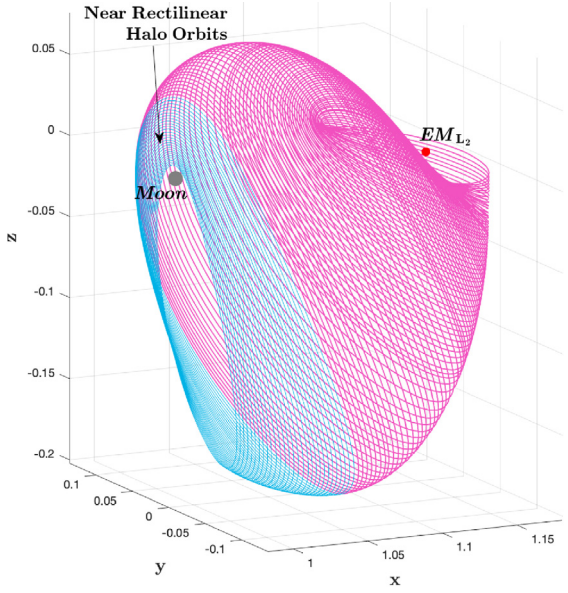

Fig. 1. L_2 Halo family in the Earth-Moon system.

of v_i, the faster a perturbed Halo orbit would deviate from its nominal path. In the Earth-Moon system, the NRHOs are defined as the set of Halo orbits whose stability indices are no larger than 2 in modulus (Guzzetti et al., 2017).

2.2.2. Quasi-satellite orbits

QSOs, also known in the literature as retrograde relative or distant retrograde orbits, have attracted sustained attention since 1969, when their linear stability was first confirmed by Hénon in his numerical investigations (Hénon, 1969). As stable periodic orbits around the secondary mass of a restricted three-body system, QSOs have been considered as potential science orbits for multiple deep-space missions, including ESA's DePhine (Oberst et al., 2018) and NASA's JIMO (Xu and Xu, 2009a). More recently, JAXA has proposed the adoption of low-altitude QSOs around Phobos for the scientific investigations of the Martian Moons eXploration mission (MMX) to be launched in 2024 (Baresi et al., 2021). Five QSO orbits are currently under investigation for the MMX proximity phase, whereby the dynamical and geophysical environment of Phobos will be explored in great detail. As shown in Fig. 2, periodic orbits of the QSO family can reach extremely low altitudes with respect to the surface of the Martian moon, especially near the Mars and anti-Mars directions. Nevertheless, QSOs remain linearly stable across all altitude values as the maximum norm of their stability index $|v_i|_{max}$ is never found to be greater than one.

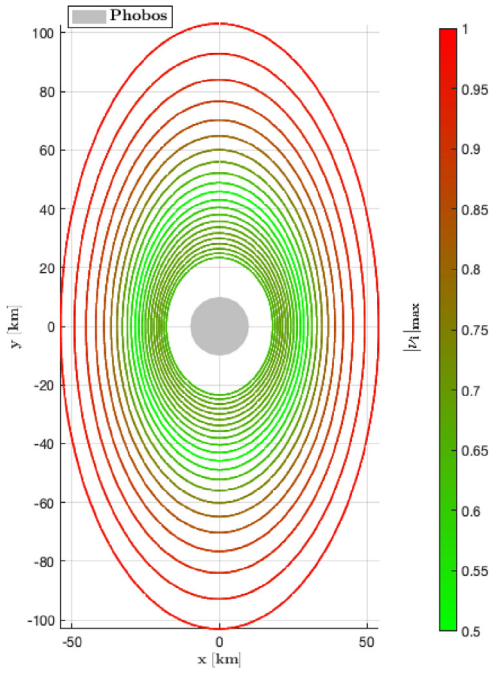

Fig. 2. QSOs around Phobos.

2.3. Linear target point approach

Although both NRHOs and QSOs display either no or little instabilities, station-keeping maneuvers are in order to nullify linearization errors and external perturbations (Guzzetti et al., 2017; Baresi et al., 2021). Amongst other techniques (Shirobokov et al., 2017), the TPA method by Howell and Pernicka (1993) emerged as a simple and elegant solution to a linear-quadratic regulator problem whereby impulsive maneuvers are implemented in order to nullify the error between the estimated and reference orbit of a spacecraft mission. To illustrate this approach, let t_c be the epoch where a corrective maneuver needs to be implemented. The maneuver magnitude and direction is then obtained by minimizing the following cost function:

$$J = \Delta \mathbf{v}^T Q \Delta v + \sum_{i=1}^{n} p_{t_i}^T R_i p_{t_i}, \tag{7}$$

where the superscript T denotes transpose; $\Delta \mathbf{v}$ denotes a maneuver at t_c; p_{t_i} denotes the predicted position residual at a specified future epoch t_i; the symmetric positive definite matrix Q is the weighting matrix of the control energy required by the maneuver; the symmetric positive semi-definite R_i is the weighting matrix of the position deviation at t_i. In the TPA, $\{t_i\}_{i=1}^n$ are called the target times and thus, the spacecraft's positions at future times t_i along a nominal orbit are called the target points (TPs). In practice, the orbit determination epoch t_0 is marked as the starting time of a TPA process. Hereby, t_0, t_c, and $\{t_i\}_{i=1}^n$ are collectively referred to as TPA epochs.

Assuming that the deviations from a nominal trajectory are within the limits of linear perturbation theory, then the position errors at each target time t_i can be approximated using the state transition matrices $\Phi(t_i, t_0)$ and $\Phi(t_i, t_c)$:

$$\mathbf{p}_{t_i} = B_{t_i,t_c} \Delta v + B_{t_i,t_0} e_{t_0} + A_{t_i,t_0} p_{t_0} \tag{8}$$

where $\mathbf{p}_{t_0}$ and e_{t_0} denote the position and velocity residuals at t_0 respectively. The capital letters A and B represent the 3×3 submatrices of a 6×6 state transition matrix Φ, which is partitioned as

$$\Phi = \begin{bmatrix} A & B \\ C & D \end{bmatrix}.$$

By substituting Eq. (8) into Eq. (7) and solving for $\Delta \mathbf{v}$ to minimize the cost function J, the optimal Δv can be derived analytically as:

$$\Delta \mathbf{v} = \gamma \sum_{i=1}^{n} \left[\boldsymbol{\alpha}_i p_{t_0} + \boldsymbol{\beta}_i e_{t_0}, \right] \tag{9}$$

where

$$\begin{aligned} \gamma &= -\left[Q + \sum_{i=1}^{n} B_{t_i,t_c}^T R_i B_{t_i,t_c} \right]^{-1}, \\ \boldsymbol{\alpha}_i &= B_{t_i,t_c}^T R_i A_{t_i,t_0}, \\ \boldsymbol{\beta}_i &= B_{t_i,t_c}^T R_i B_{t_i,t_0}. \end{aligned} \tag{10}$$

Once TPA epochs and weighting matrices are determined, an optimal TPA maneuver $\Delta \mathbf{v}$ is solely dependant on the state residuals at t_0. It is remarkable that the analyt-

ical expression of Δv in the linear TPA is deduced based on a linear perturbation assumption and the leveraging of STMs. To remedy this deficiency and achieve more accurate optimal maneuvers, a high-order TPA is first proposed in the next section.

3. Methodology

In this section, a high-order TPA method is first introduced, thereby enabling the calculation of accurate station-keeping maneuvers in chaotic nonlinear environments. Subsequently, a TPA-based stationkeeping strategy is proposed by taking advantage of the periodicity of a periodic orbit. The approach to OD epoch selection is developed and explained as well. Combining the methods above, a stochastic optimization algorithm in search of fuel-optimal and error-robust TPA parameters is elaborated.

3.1. High-order target point approach

In this subsection, a high-order TPA is proposed, in which a maneuver map is built to efficiently calculate optimal maneuvers by means of polynomial evaluations. The map is constructed with DA-based partial inversion techniques and the corresponding procedures are as follows. Let the gradient of cost function J be a function of the optimal maneuver $\Delta\mathbf{v}$ and the state X_0 at t_0 as noted in the linear case: $\nabla J = \nabla J(\Delta v, X_0)$. A manifest solution of this equation is $\left(\mathbf{0}_{3\times1}, X_0^{Ref}\right)$, where X_0^{Ref} denotes the reference state at t_0. Based on this trivial solution, the computation of other solutions $\left(\Delta v^*, X_0^*\right)$ can be achieved using the nonlinear impulsive maneuver solver proposed in the authors' previous work (Fu et al., 2020). Subsequently, the increment of ∇J at a given zero $\left(\Delta v^*, X_0^*\right)$ can be acquired by expanding ∇J as a high-order polynomial map, resulting in:

$$\delta\nabla J = \mathcal{T}_{\delta\nabla J}(\delta\Delta v, \delta X_0) \tag{11}$$

where $\delta\nabla J$ represents the increment of ∇J at the expansion point $\left(\Delta v^*, X_0^*\right)$, $\mathcal{T}_{\delta\nabla J}(\delta\Delta v, \delta X_0)$ denotes a high-order polynomial map of $\delta\nabla J$ with respect to $(\delta\Delta v, \delta X_0)$ expanded at the expansion point, and $\delta X_0 = X_0 - X_0^{Ref}$. Eq. (16) can be rewritten as

$$\begin{bmatrix} \delta\nabla J|_{\Delta v} \\ \delta\nabla J|_{X_0} \end{bmatrix} = \begin{bmatrix} \mathcal{T}_{\delta\nabla J|_{\Delta v}}(\delta\Delta v, \delta X_0) \\ \mathcal{T}_{\delta\nabla J|_{X_0}}(\delta\Delta v, \delta X_0) \end{bmatrix} \tag{12}$$

where the subscripts $\delta\nabla J|_{\Delta v}$ and $\delta\nabla J|_{X_0}$ denote the gradient components with respect to Δv and X_0, respectively. $\mathcal{T}_{\delta\nabla J|_{\Delta v}}$ and $\mathcal{T}_{\delta\nabla J|_{X_0}}$ are the corresponding submaps.

For the submap $\mathcal{T}_{\delta\nabla J|_{\Delta v}}(\delta\Delta v, \delta X_0)$, a partial inversion yields:

$$\delta\Delta\mathbf{v} = \mathcal{T}_{\delta\Delta\mathbf{v}}(\delta\nabla J|_{\Delta v}, \delta X_0) \tag{13}$$

Enforcing $\delta\nabla J|_{\Delta v} = \mathbf{0}$ for $\forall\delta X_0$ in Eq. (13) then outputs

$$\delta\Delta\mathbf{v} = \mathcal{T}_{\delta\Delta\mathbf{v}}(\delta X_0) \tag{14}$$

Substituting Eq. (14) into $\Delta\mathbf{v} = \mathcal{T}_{\Delta\mathbf{v}}(\delta\Delta v)$ finally gives:

$$\Delta\mathbf{v} = \mathcal{T}_{\Delta v}(\delta X_0) \tag{15}$$

which is a maneuver map establishing the relationship between an optimal high-order maneuver $\Delta\mathbf{v}$ and arbitrary δX_0 errors within the convergence domain of Eq. (15).

A noteworthy strength of this approach is that it avoids repeated computations for a relatively large set of initial errors in a certain domain of interest. That is, once a maneuver map is established for a selected expansion point, the optimal manuevers of points in the neighborhood of the expansion point can be efficiently calculated via simple polynomial evaluations. As a critical operation to build this maneuver map, the partial inversion of a polynomial map is based on the work of Berz (Berz, 1999), where the inversion of polynomials is reduced to the solution of an equivalent fixed point problem. This problem can be readily solved in the DA setting through a multiple evaluation of the associated fixed point operator. The procedure to obtain the fixed point operator relies on the inverse of the linear part of the map to be inverted. Therefore, as long as no singularities occur in the linear solution, i.e. the linear TPA approach, high-order maneuver maps can always be achieved.

To further demonstrate the accuracy of the proposed high-order TPA method in maneuver calculation, an eigenvector-based multivariate analysis (Fu et al., 2020) is conducted for the NRHO orbit hereby referred to as Candidate #2 in Table 1. Two scaled principal directions for the accuracy analysis, $\bar{\mathbf{v}}_1$ and $\bar{\mathbf{v}}_2$, are determined by a singular value decomposition of the Jacobian matrix from Eq. (15). The nonlinear impulsive maneuver solver (later referred to as "nonlinear TPA"), which is developed from a DA-based high-order Newton's method and elaborated by Fu et al. (2020), is employed to solve for the accurate reference maneuvers for comparison. The process of this nonlinear maneuver solver is illustrated in Fig. 3. For simplicity, only two target points are shown in the illustration and navigation errors are neglected. Two trajectories of interest, the reference and true trajectories, are propagated to provide the position deviations for the cost function J in Eq. (7). Note that an initial state error $\boldsymbol{\epsilon}_{t_0}$ is added to the state of the reference trajectory in order to produce a true trajectory that differs from the desired orbital path. Following the nonlinear propagation of both trajectories, the gradient of J with respect to $\Delta\mathbf{v}, \nabla J$, is calculated using the embedded differentiation capabilities of DA. To search for an accurate value of Δv, the following high-order Newton's iteration is employed

$$\Delta\mathbf{v}_{k+1} = \Delta v_k - \mathcal{T}^{-1}_{\delta\nabla J}(\delta\nabla J) \tag{16}$$

where the symbol δ represents the increment of a variable, and $\mathcal{T}^{-1}_{\delta\nabla J}$ stands for the inverse of the high-order polynomial map $\delta\nabla J = \mathcal{T}_{\delta\nabla J}(\delta\Delta\mathbf{v})$. The refined maneuver $\Delta v_{H.O.T}$ acquired from each Newton's iteration is applied

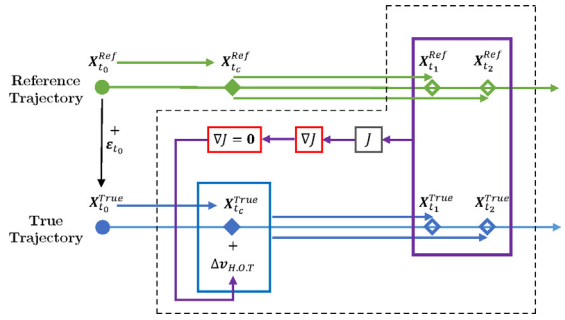

Fig. 3. Illustration of Nonlinear Maneuver Solver.

to update the guess of the optimal maneuver at t_c and added to the state of the true trajectory. By repeating the above procedures (which are enclosed by dashed lines in Fig. 3) until the magnitude of $\delta\nabla J$ reaches a prescribed epsilon, the accurate optimal maneuver is acquired.

By means of nonlinear TPA, high-order TPA, and linear TPA, the magnitude of maneuvers calculated from three TPA methods and their differences are respectively shown in Fig. 4 and Fig. 5. The TPA parameters adopted to generate two contour plots correspond to the third row in Table 5. In Fig. 4, it is noticeable that the contours of $||\Delta\mathbf{v}||$ for the linear TPA are concentric circles of the origin, since they are plotted along the scaled principal directions. In the middle subplot where the maneuvers of the nonlinear TPA are presented, contours remain concentric for small $||\Delta v||$. As the magnitude of $||\Delta v||$ increases, the corresponding contours gradually deform due to the nonlinearity of the CRTBP. For contours generated by the high-order TPA, they hold similar shapes in comparison with those of the nonlinear TPA. To further compare the accuracy of maneuvers between the three TPA methods, maneuver differences of the high-order TPA and linear TPA with respect to the references are calculated and presented on a logarithmic scale in Fig. 5. As expected, both high-order TPA and linear TPA can maintain a high accuracy in a small neighborhood of the expansion point. However, as the magnitude of state residuals increases along the two principal directions, the error of maneuvers from the linear TPA is observed to increase drastically as opposed to the one obtained from the high-order TPA. In the domain of interest, a maximum error of 25 percent is reached by the maneuvers calculated from linear TPA, while the maximum error from high-order TPA is merely around 1E-4 m/s.

3.2. TPA-based stationkeeping strategy for periodic orbits

3.2.1. Stationkeeping process

Generally, in a complete stationkeeping process, three trajectories of interest are taken into account, namely the reference trajectory, the true trajectory, and the determined trajectory. Stationkeeping epochs, including the orbit injection (OI) epoch, orbit determination (OD) epochs, and maneuver execution (EX) epochs, are crucial to the performance of a stationkeeping strategy. In addition, the uncertainties existing in a stationkeeping process are supposed to be modeled properly. In this section, a stationkeeping strategy incorporating all these key factors is designed and further streamlined by taking advantage of the orbital periodicity and the property of TPA.

The stationkeeping process of a period orbit based on the TPA is illustrated in Fig. 6. In order to precisely simulate this process, three major types of errors, including the OI error ϵ_{OI}, OD error ϵ_{OD}, and EX error ϵ_{EX}, are modeled and generated with zero-mean Gaussian distributions. Let $\mathbf{X}^{Ref}, X^{True}$, and X^{Det} denote the state of reference trajectory, true trajectory, and determined trajectory respectively. It is assumed that the orbit injection epoch t_{OI} is the same as the first orbit determination epoch $t_{OD}^{(1)}$. Thus, an OI error ϵ_{OI} can be added directly to the state of reference trajectory at t_{OI} to generate $X_{OD^{(1)}}^{True}$, the true state at $t_{OD}^{(1)}$. Similarly, the state of determined trajectory at $t_{OD}^{(1)}, X_{OD^{(1)}}^{Det}$, can be achieved by adding an OD error ϵ_{OD} to $X_{OD^{(1)}}^{True}$. Once the two aforementioned states are determined, the true trajectory is propagated to the first maneuver epoch $t_{EX}^{(1)}$. The resulting true state, $X_{EX^{(1)}}^{True}$, will be corrected by an optimal maneuver $\Delta\mathbf{v}_{(1)}$, which is calculated with the state residual between the determined state and reference state at $t_{OD}^{(1)}$

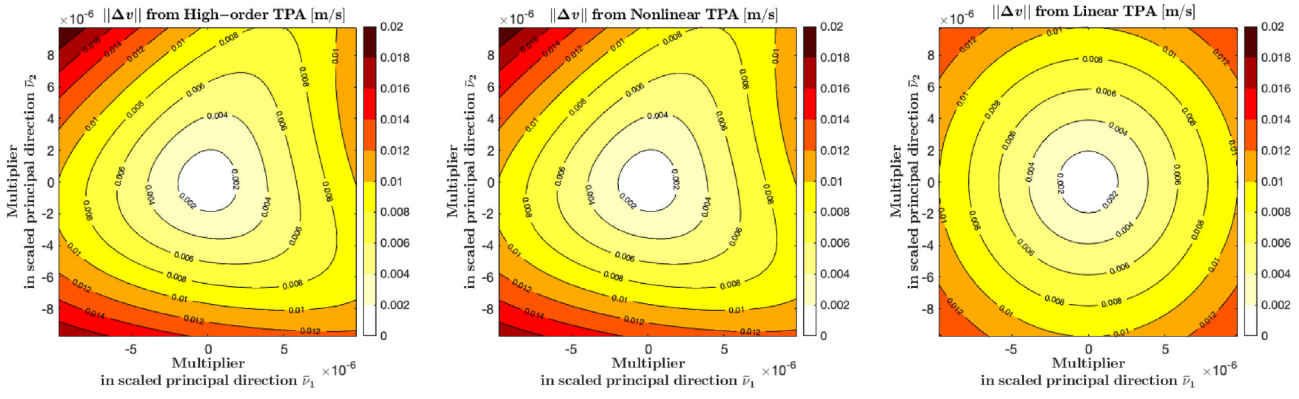

Fig. 4. Maneuvers calculated from three TPA methods.

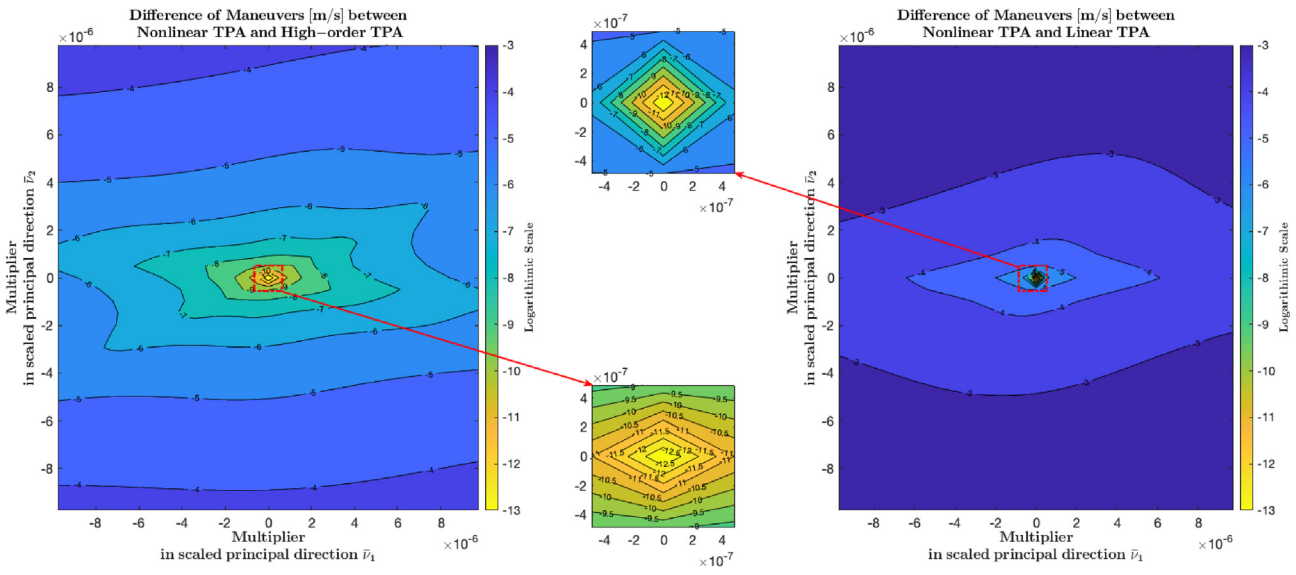

Fig. 5. Difference of maneuvers between three TPA methods.

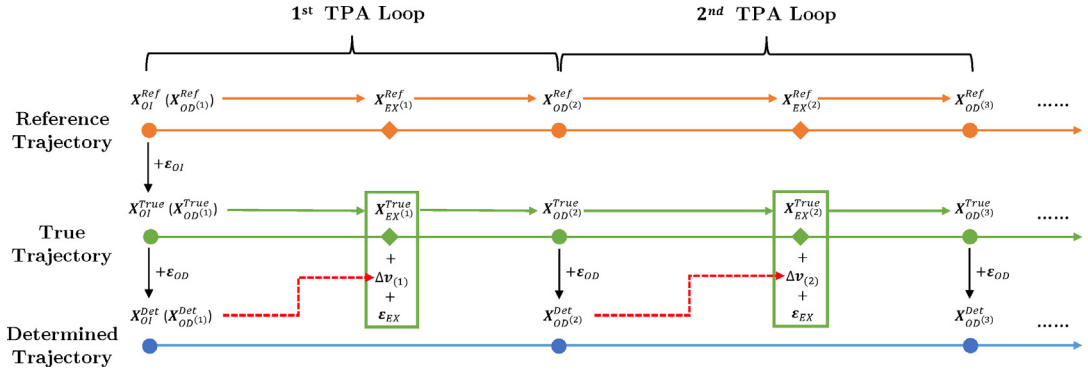

Fig. 6. Stationkeeping Process based on TPA.

and later perturbed by an EX error ϵ_{EX}, and then propagated till the next OD epoch. The reference trajectory is also propagated to the next OD epoch and the reference states at $t_{EX}^{(1)}$ and $t_{OD}^{(2)}$ will be recorded. All the above operations between two consecutive OD epochs are repeated until the end of this stationkeeping process. It has to be remarked that, the initial assumption about the identical placement of OI epoch and the first OD epoch won't necessarily lead to a loss of generality. Even if an interval is arranged between the two epochs, the accurate states of both reference and true trajectories at $t_{OD}^{(1)}$ are still achievable via propagation. Such an arrangement is tantamount to a variation of the OI error under our current assumption, which can be handled within this stationkeeping process.

The strategy described above already provides a general framework for TPA-based stationkeeping processes. Furthermore, the stationkeeping procedures can be rendered even more efficient by exploiting the orbital periodicity and the property of TPA. Finite states generated within one orbital period can sufficiently provide the reference state at any stationkeeping epoch by implementing interpolation techniques. Moreover, the advantage gained in maneuver calculation is also significant when the orbital periodicity is exploited in this TPA based stationkeeping strategy. Let the interval between two consecutive OD epochs be defined as a TPA loop. It is generally assumed that a long-term TPA stationkeeping process is composed of multiple TPA loops, inside of which the TPA epochs are relatively fixed, i.e. the interval from an OD epoch to an EX epoch or to TP epochs is invariant for any TPA loop. When the length of a TPA loop is restricted to a multiple of the orbital period, the placement of crucial TPA epochs will remain fixed on a reference periodic orbit. This observation justifies the adoption of one set of TPA parameters for all the TPA loops. Therefore, once STMs or a high-order maneuever map is calculated using the TPA epochs in one TPA loop, they can be reused in the remaining station-keeping simulation. By removing a repeated and time-consuming STM propagation or maneuver map calculation, the efficiency of this stationkeeping strategy is further improved.

3.2.2. Selection of orbit determination epoch

The selection of OD epoch directly influences the performance of a stationkeeping strategy. Due to the possible proximity of a periodic orbit to a primary body, uncertainty in an OD process can be increased dramatically via orbit propagation and induce a considerable maneuver cost. In a worst-case scenario, an inappropriate OD position can even make a stationkeeping strategy fail. To minimize the growth of OD errors in this TPA-based stationkeeping process, the OD epoch is determined by conducting a sensitivity analysis based on the convergence radius of a stroboscopic map. Details of this analysis are provided as follows.

Reference points distributed evenly along a periodic orbit are extracted initially. For each reference point, a stroboscopic map, i.e., a high-order expansion of an ODE flow propagated for one orbital period, is constructed:

$$\delta \mathbf{X}_f = \mathcal{T}_{\delta X_f}(\delta X_0) \tag{17}$$

where $\delta \mathbf{X}_0$ denotes the perturbation exerted at the initial reference state and δX_f denotes the final state residual. A linear quadratic form is established subsequently to quantify the state deviation after one orbital period:

$$J_f = \delta \mathbf{X}_f^T W \delta X_f \tag{18}$$

where $W = diag\left(w_{pos}, w_{pos}, w_{pos}, w_{vel}, w_{vel}, w_{vel}\right)$ denotes a diagonal matrix including weights for position and velocity elements respectively. By substituting Eq. (17) into Eq. (18), the relationship between J_f and perturbation at each reference state $\delta \mathbf{X}_0$ is established, i.e., $J_f = J_f(\delta X_0)$. Thereafter, the convergence radius of map $J_f(\delta X_0)$ is further estimated and employed to determine the sensitivity of each reference point.

The convergence radius of a polynomial map is defined as the size of the uncertainty set that is mapped by the polynomial with a requested accuracy. The variation between the convergence radii of stroboscopic maps can provide an evident indication of the tolerance to errors for the corresponding reference points. A larger convergence radius represents a lower sensitivity to uncertainties and thus, the corresponding reference state is more eligible for an OD operation to minimize the influence from navigation errors. In addition, the convergence radius of a Taylor polynomial map can be readily estimated with an embedded function *convRadius* in DA toolbox (Wittig et al., 2015), which further streamlines the aforementioned analysis. Specifically, only two inputs are required by this function: one is a given DA polynomial map, another is a demanded tolerance ϵ.

An example is offered hereby to illustrate the selection of an OD epoch for the stationkeeping of a NRHO. The selected NRHO is labeled as Candidate #1 in Table 1. As shown in Fig. 7, reference points, which are marked by empty blue circles, are chosen to be distributed evenly along the candidate NRHO. Red arrows indicate the orbit's clockwise direction of motion in the *yoz* projection. A phase angle θ is defined to differentiate the reference points and the zero phase angle corresponds to the apolune of this NRHO. Without losing generality, the weight matrix in Eq. (18) is further formulated as $W = diag\left(1, 1, 1, \frac{w_{vel}}{w_{pos}}, \frac{w_{vel}}{w_{pos}}, \frac{w_{vel}}{w_{pos}}\right)$. A requested tolerance ϵ is set to 10^{-6} and the convergence radius of map $J_f(\delta \mathbf{X}_0)$ for each reference point is calculated. As shown in Fig. 8, the smallest convergence radii always appear when the phase angle is close to π, i.e., the perilune of the candidate NRHO, regardless of the ratio $\frac{w_{vel}}{w_{pos}}$. Such a fact is reasonable since the dynamics in the vicinity of the Moon changes more drastically than the other regions, and a same level of errors can experience a larger augmentation after one-period propagation. Hence, the maps generated by the corresponding reference states are more sensitive to initial errors and allow for a smaller convergence radii. In contrast, the largest convergence radii are found near the apolune, where the gravitational attraction from the Moon is much weaker. A similar finding on the sensitivity of a NRHO is reported by Jenson and Scheeres (2021b) when the tensor eigenpairs are exploited to quantify the nonlinearity of the Earth-Moon CRTBP model. In summary, to minimize the growth of OD errors, the apolune is selected as the OD position for the stationkeeping of the candidate NRHO.

3.3. Stochastic optimization of TPA parameters

By means of the stationkeeping strategy elaborated in last subsection, the performance of a TPA stationkeeping process is predominantly dependent upon several crucial TPA parameters, including TPA epochs and the weighting matrices of the TPA cost function J. Generally, these parameters are manually tuned through trial and error. Such a process could be fairly lengthy and the acquired TPA parameters are always problem-specific and non-optimal. A possible solution is to apply global optimization techniques to search for optimal TPA parameters as proposed by Dei Tos and Baresi (2020).

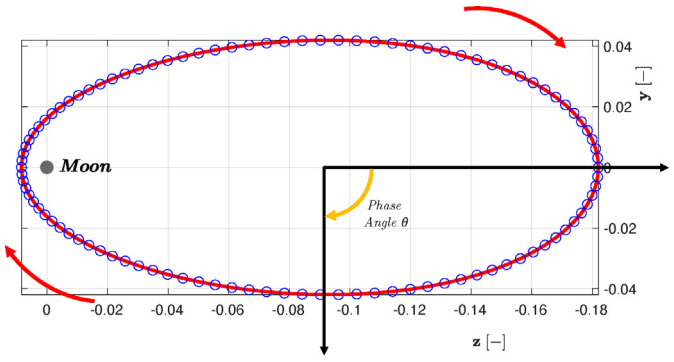

Fig. 7. Reference Points Distributed along a Candidate NRHO.

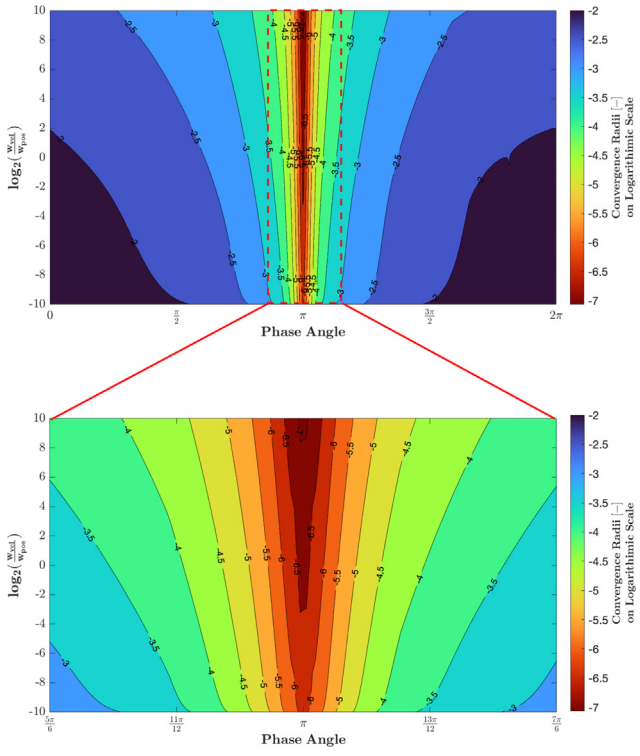

Fig. 8. Convergence Radii of Map $J_f(\delta \mathbf{X}_0)$ generated along a Candidate NRHO.

Due to the existence of uncertainties in stationkeeping problems, the effectiveness of a stationkeeping strategy is always investigated with a posterior analysis, where errors from different sources are randomly sampled in a large-scale MC trial. Such an analysis is a widely adopted approach to properly test the robustness of a stationkeeping method in handling stochasticity. Hence, in this section, an algorithm to acquire error-robust optimal TPA parameters is proposed by embedding MC simulations in a global optimization process. The determination of search space and design variables used in the global optimization will be fully discussed before moving to a detailed description of the algorithm.

3.3.1. Search space and design variables

To reduce the search space of optimization, two assumptions are respectively made about the structure of weighting matrices and the number of TPs. Previous TPA research (Dei Tos and Baresi, 2020) has shown that the driven factor for the selection of weighing matrices is the ratio between Q and R_i, rather than their independent values. Therefore, Q is set to a 3×3 identity matrix I and only R_i are optimized. It is also assumed that R_i are diagonal matrices which can be expressed with $R_i = 10^{\rho_i} I$. Moreover, two TPs are assumed in this work, which satisfies the minimum requirement for the number of TPs and meanwhile conduces an understanding of the influence from an extra TP. In addition to the assumptions above, another two decisions are taken for the determination of the search space. By means of the stationkeeping strategy discussed in the previous subsection, the OD epoch is selected at the least sensitive position of a candidate orbit to minimize the growth of OD errors. The length of each TPA loop, which is denoted by T_{Loop}, is selected as a multiple of the orbital period of a candidate orbit. It follows that the search space is effectively reduced to five dimensions.

A further definition of design variables is necessary after the five-dimension search space is determined. There is no doubt that ρ_1 and ρ_2 are the two design variables representing the weighting matrices. As for the rest three design variables related with TPA epochs, two constraints on TPA epochs have to be taken into account in terms of TPA itself. By definition, a 1st TP epoch (t_{TP1}) should always be located ahead of a corresponding 2nd TP epoch (t_{TP2}). In addition, the influence of the $(i+1)$ th maneuver on the TP states in the ith TPA loop should be minimized. Thus, the ith t_{TP1} epoch should be placed ahead of the $(i+1)$ th maneuver epoch. Based on the two constraints, three design variables are defined and illustrated in Fig. 9. Let $\Delta t_c, \Delta t_g$, and Δt_{TP} denote the interval between the ith OD epoch and ith EX epoch, the interval between the ith t_{TP1} and $(i+1)$ th maneuver epoch, and the interval between two TPs, respectively. By restricting Δt_c and Δt_g within a domain of $(0, T_{Loop})$, the two constraints above will be automatically satisfied. In comparison, the domain of Δt_{TP} is not influenced by any constraints and is set to vary between zero and six orbital periods. Consequently, such a definition of design variables can definitely determine all the TPA epochs in a stationkeeping process, and meanwhile enable the application of an unconstrained global optimization algorithm.

3.3.2. Monte-Carlo embedding

By virtue of the five aforementioned design variables, a stochastic optimization algorithm with embedded MC simulation is formulated to search for error-robust TPA parameters. The performance of a given set of design variables will be evaluated by the statistics from stationkeeping processes, which are initialized by a considerate amount of OI states sampled on the true trajectory. In order to make a differentiation, the mark $\{\cdot\}$ is hereby used to denote a set of states, e.g. $\{\mathbf{X}_{OI}^{True}\}$ denotes a set of true states at OI epoch, while X_{OI}^{True} denotes one single true OI state. To accurately demonstrate the error robustness of TPA parameters, the number of MC samples is supposed to be sufficiently large. In a station-keeping research, such a requirement inevitably leads to numerically intensive orbit propagations. The ordinary solution of using numerical integration can hardly qualify, especially considering the frequent evaluation of the fitness function in a global optimization approach. Such an issue can be efficiently tackled by means of the high-order expansion of the ODE flow as shown in the following.

The automatic high-order expansions of ODE flows can be achieved by performing a numerical integration of an ODE in the DA framework. This is a result of numerical

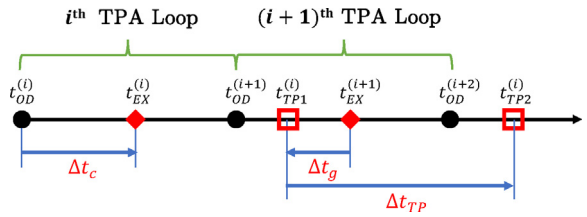

Fig. 9. Design Variables related with TPA Epochs.

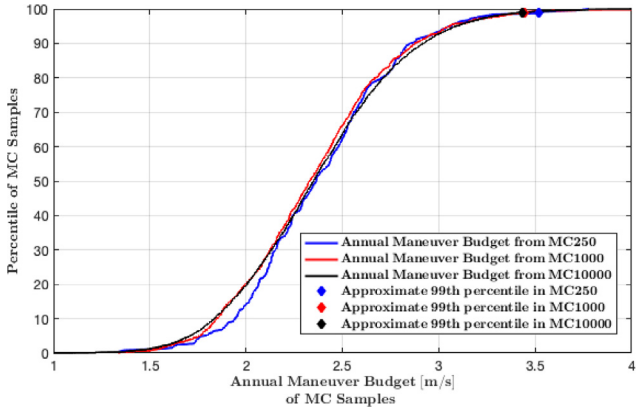

Fig. 10. Statistics on annual maneuver budget from MC simulations with different sample sizes. Stationkeeping configurations are detailed in the following section and the TPA parameters adopted for this MC simulations correspond to the third row in Table 4.

integration methods being based on algebraic operations (e.g. differentiation and function evaluation) that can be all handled by DA. A strength of the DA-based integration is that the expansion of ODE solutions can be calculated against either the initial condition and/or any parameter of the dynamics. Such a technique has been adopted in different astrodynamics problems, with its accuracy and efficiency widely validated (Armellin et al., 2010a; Armellin et al., 2010b; Wittig et al., 2015). Accordingly, once the station-keeping epochs of one TPA loop are determined, the following two high-order ODE expansions can be formulated:

$$X_{EX} = \mathcal{T}_{X_{EX}}(\delta X_{OD}), \tag{19a}$$

$$X_{OD} = \mathcal{T}_{X_{OD}}(\delta X_{EX}). \tag{19b}$$

Eq. (19a) links state deviations at the nominal OD epoch to state deviations (from the reference periodic orbit) at the maneuver execution epoch. As usual, if $\delta X_0 = 0$, then $X_{EX} = X_{EX}^{ref}$. Similarly, Eq. (19b) maps state deviations X_{EX}^{ref} at the maneuver execution epoch to state deviations at the next OD epoch. Owing to the periodicity of the reference trajectory, the two maps can be chained together and combined with the high-order maneuver map to propagate a very large number of sample trajectories over an arbitrary number of TPA loops. The key advantage is that, by virtue of these two high-order ODE flow expansions, the propagation of the true orbits is reduced to a fast polynomial evaluation. Sufficiently large input state residual sets $\{\delta \mathbf{X}_{OD}\}$ and $\{\delta X_{EX}\}$ can be readily handled and thus, sufficient MC samples are attainable, which assures the validity of acquired optimal TPA parameters. As shown in Fig. 10, MC simulations with three different sample sizes are executed and the annual maneuver budgets of all samples are presented for each simulation individually. It is noteworthy that a sample size of 1,000 is capable of offering a promising trade-off between simulation run-time and the accuracy of statistical approximation.

3.3.3. Fitness function

The fitness function of the proposed stochastic optimization using high-order ODE flows is elaborated in Algorithm 1. As described in previous subsection, five design variables of the fitness function are determined as $\rho_1, \rho_2, \Delta t_c, \Delta t_g$, and Δt_{TP}. Additionally, several other parameters have to be provided to the fitness function as well. The number of TPA loops N_{loop} for a specified stationkeeping duration is calculated by

$$N_{loop} = ceil\left((t_{end} - t_{OI})/T_{Loop}\right) \tag{20}$$

where t_{OI} and t_{end} denote the starting and ending epoch of a stationkeeping process respectively, and *ceil* represents an operation in which a positive value is rounded to its nearest integer greater than or equal to itself. N_{loop} will further determine the size of OI error set $\{\epsilon_{OI}\}$, OD error set $\{\epsilon_{OD}\}$, and EX error set $\{\epsilon_{EX}\}$. These three error sets are modeled and pre-generated with zero-mean Gaussian distribution, i.e. $\epsilon_{OI} \sim \mathcal{N}(0, \sigma_{OI}^2), \epsilon_{OD} \sim \mathcal{N}(0, \sigma_{OD}^2), \epsilon_{EX} \sim \mathcal{N}(0, \sigma_{EX}^2)$, where $\sigma_{OI}^2, \sigma_{OD}^2$, and σ_{EX}^2 are the covariances of the OI, OD, and EX uncertainties respectively. Thus far, the input of the fitness function is clearly defined. The fitness evaluation of a TPA parameter set starts with the calculation of stationkeeping epochs, which relies on the previously defined quantities as follows:

$$\begin{aligned} t_{EX}^{(i)} &= t_{OD}^{(i)} + \Delta t_c, \\ t_{TP1}^{(i)} &= t_{EX}^{(i)} + T_{Loop} - \Delta t_g, \\ t_{TP2}^{(i)} &= t_{TP1}^{(i)} + \Delta t_{TP}, \\ t_{OD}^{(i+1)} &= t_{OD}^{(i)} + T_{Loop}. \end{aligned} \tag{21}$$

Once the station-keeping epoch sequence is constructed, the two high-order ODE flows can be established using the TPA epochs of any TPA loop. A subsequent operation is to calculate either STMs for linear TPA or build a maneuver map for high-order TPA, thus preparing the algorithm for a whole station-keeping simulation. A maximum tolerance for position deviation, Δd_{max}, is introduced to define a station-keeping failure, i.e., whenever the position residual of a true trajectory reaches a prescribed tolerance during a station-keeping process, the corresponding MC run will be terminated and labeled as a failure. The number of all failed MC runs N_{fail} will be recorded for a

given set of TPA parameters. Once an MC-embedded station-keeping simulation is completed, a data set of the total maneuver cost of each eligible MC run, $\{||\Delta \mathbf{v}||_{total}\}$, is generated. The approximated 99-th percentile of the elements in $\{||\Delta v||_{total}\}$, which is denoted by $||\Delta v||^{99}_{total}$, is employed as a statistical indicator of the station-keeping maneuver budget. In this work, the fitness value $J_{S/K}$ is defined as

$$J_{S/K} = ||\Delta \mathbf{v}||^{99}_{total} + N_{fail} \tag{22}$$

which includes both the stochastic station-keeping cost and the convergence performance of a given set of design variables.

employing the proposed methodology. Stationkeeping configurations and global optimization set-up are introduced and stationkeeping results and findings are subsequently discussed.

4.1. Stationkeeping analysis of candidate NRHOs

Two NRHOs of interest, the two candidate NRHOs of LOP-G mission (Williams et al., 2017), are selected as test cases. Both LOP-G candidates are carefully selected to guarantee specific resonance ratios between the lunar synodic cycle (roughly 29.53 day) and their corresponding orbital periods. Detailed orbital parameters of the candidate NRHOs of interest are provided in Table 1.

Algorithm 1. Fitness function of the stochastic optimization of TPA parameters

function FITNESS_SK_TPA$\left(\rho_1, \rho_2, \Delta t_c, \Delta t_g, \Delta t_{TP}, \mathbf{X}^{Ref}_{OI}, N_{loop}, \{\boldsymbol{\epsilon}_{OI}\}, \{\boldsymbol{\epsilon}_{OD}\}, \{\boldsymbol{\epsilon}_{EX}\}\right)$
  Construct S/K epoch sequence: $t^{(i)}_{OD}, t^{(i)}_{EX}, t^{(i)}_{TP1}, t^{(i)}_{TP2}$. ▷See Eq. (21)
  Build high-order ODE flows: $\mathcal{T}_{\mathbf{X}_{EX}}(\delta X_{OD}), \mathcal{T}_{X_{OD}}(\delta X_{EX})$ ▷See Eq. (19)
  if Linear TPA **then**
    Calculate STMs $\Phi(t_{EX}, t_{OD})$ and $\Phi(t_{TPi}, t_{OD})$ ▷See Eq. (8)
  else if High-order TPA **then**
    Build maneuver map $\Delta \mathbf{v} = \mathcal{T}_{\Delta v}(\delta X_{OD})$ ▷See Eq. (15)
  end if
  OI: $\{X^{True}_{OI}\} \leftarrow \left\{X^{Ref}_{OI}\right\} + \{\boldsymbol{\epsilon}_{OI}\}$, $\left\{X^{True}_{OD^{(1)}}\right\} \leftarrow \{X^{True}_{OI}\}$
  while $i \leqslant N_{loop}$ & $\left\{\delta \mathbf{X}^{True}\right\} \leqslant \Delta d_{max}$ **do**
    OD: $\left\{\mathbf{X}^{Det}_{OD^{(i)}}\right\} \leftarrow \left\{X^{True}_{OD^{(i)}}\right\} + \{\boldsymbol{\epsilon}_{OD}\}$
    Propagate true trajectory: $\left\{\mathbf{X}^{True}_{EX^{(i)}}\right\} \leftarrow \mathcal{T}_{X_{EX}}\left(\left\{\delta X^{True}_{OD^{(i)}}\right\}\right)$
    if Linear TPA **then**
      $\{\Delta \mathbf{v}_{(i)}\} = f\left(\Phi(t_{EX}, t_{OD}), \Phi(t_{TPi}, t_{OD}), \left\{\delta X^{Det}_{OD^{(i)}}\right\}\right)$
    else if High-order TPA **then**
      $\{\Delta \mathbf{v}_{(i)}\} = \mathcal{T}_{\Delta v}\left(\left\{\delta X^{Det}_{OD^{(i)}}\right\}\right)$
    end if
    $\{\Delta \mathbf{v}_{(i)}\} \leftarrow \{\Delta v_{(i)}\} + \{\boldsymbol{\epsilon}_{EX}\}$
    Execute Maneuver: $\left\{\mathbf{X}^{True}_{EX^{(i)}}\right\} \leftarrow \left\{X^{True}_{EX^{(i)}}\right\} + \left\{\left[\mathbf{0}_{3\times 1}; \Delta v_{(i)}\right]\right\}$
    Propagate true trajectory: $\left\{\mathbf{X}^{True}_{OD^{(i+1)}}\right\} \leftarrow \mathcal{T}_{X_{OD}}\left(\left\{\delta X^{True}_{EX^{(i)}}\right\}\right)$
  end while
  Number of failed MC runs: N_{fail}
  Total maneuver cost of eligible MC runs: $\left\{||\Delta \mathbf{v}||_{total}\right\} \leftarrow \left\{\sum ||\Delta v_{(i)}||\right\}$
  Fitness value: $J_{S/K}$ ▷See Eq. (22)
end function

4. Station-keeping analyses

In this section, station-keeping analyses for specific candidate NRHOs and QSOs are conducted respectively by

As illustrated in Fig. 8, the OD epoch is selected at the apolune for each candidate NRHO. Two levels of insertion and navigation errors are assumed and reported in Table 2. For a low-level accuracy, a 3σ knowledge error of 1 km in

Table 1
Parameters of candidate NRHOs.

	Perilune Radius [km]	Orbital Period [day]	Synodic Resonance	Stability Indices
Candidate #1	3227	6.563	9:2	$\nu_1 = -1.318$ $\nu_2 = 0.685$
Candidate #2	5720	7.382	4:1	$\nu_1 = -1.623$ $\nu_2 = 0.507$

Table 2
Two levels of insertion and navigation errors (3σ).

	OI error in position	OI error in velocity	OD error in position	OD error in velocity
Low-level	1 km	1 cm/s	1 km	1 cm/s
High-level	10 km	10 cm/s	10 km	10 cm/s

Table 3
Options of genetic algorithm.

Option	Value
Number of variables	5
Size of population	400
Maximum generations	300
Maximum simulation time	7 days
Crossover fraction	0.8
Creation function	Nonlinear feasible
Fitness scaling	Linear proportional
Parent selection	Tournament rule with 4 individuals
Mutation strategy	Adaptive feasible
Crossover strategy	Heuristic with coefficient $u = 1.2$

position and 1 cm/s in velocity is applied. The corresponding values are increased to ten times larger in the high level. The values reported in Table 2 are in accordance with previous research on the stationkeeping of NRHOs (Davis et al., 2017). While the navigation errors are modeled with Gaussian distributions, the maneuver execution errors are generated in a different approach, in which a fixed execution error of 0.3 cm/s is assumed and applied in a uniform random direction. In addition, a minimum maneuver threshold of 1.5 cm/s is implemented, i.e. a computed maneuver with a magnitude less than 1.5 cm/s will be canceled. By virtue of the error modeling above, three error sets, OI error set $\{\epsilon_{OI}\}$, OD error set $\{\epsilon_{OD}\}$, and EX error set $\{\epsilon_{EX}\}$, are generated before conducting an optimization. Such predetermination of stochastic errors can avoid the fluctuation in fitness values resulting from varying errors in optimization.

The genetic algorithm (GA) implemented in MATLAB is used to perform the stochastic optimization of TPA parameters. The GA optimization is performed in a parallel fashion and the corresponding algorithm options are described in Table 3. In addition, the number of MC samples used in each fitness evaluation is set to 1,000, as previously stated (c.f., Fig. 10). Such a size of MC samples is sufficient to exhibit the statistical properties of the current uncertainty modelling while assuring the error-robustness nature of the acquired TPA parameters.

4.1.1. Simulation results

Stochastic optimizations in search of optimal TPA parameters are executed for the two candidate NRHOs. Considering that a maneuver frequency of one orbital period may not be achievable due to a limited navigation capacity in practice, the length of one TPA loop is varied from one to five orbital periods. A stationkeeping duration of 52 weeks is utilized to acquire an annual maneuver cost $||\Delta \mathbf{v}||^{99}_{total}$ directly. In addition, the maximum tolerance for position deviation during stationkeeping Δd_{max} is set to 10,000 km. The optimal TPA parameters of both candidate NRHOs calculated with GA optimization are reported accordingly in Table 4 and 5, together with the annual $||\Delta v||^{99}_{total}$. In both tables, the results from 20 independent optimizations are included and all the converged optimizations have reached a predetermined fitness function tolerance of 1E-8. It is confirmed that there is no failed MC run out of 1,000 samples (i.e $N_{fail} = 0$) for all the achieved optimal TPA parameters.

It is noteworthy that a remarkable speedup is gained with the proposed optimization framework based on high-order ODE expansions, as the computation time to achieve one-generation results with the reported setup is around 20 min with 20 cores on a 2.1 GHz Intel Xeon processor. In comparison, it takes about 4 h to achieve the same simulation results by solely substituting the ODE expansions with a ordinary Runge–Kutta ODE integrator. A posterior analysis shows that the difference of $||\Delta \mathbf{v}||^{99}_{total}$ from the two aforementioned simulations is around 0.1%, which further demonstrates the accuracy of the high-order ODE expansions in trajectory propagation and guarantees the validity of the following simulation results.

As shown in both Table 4 and Table 5, the annual maneuver cost rises gradually as the length of a TPA loop increases. Such a growing tendency becomes more evident in the simulation results of the more unstable NRHO. When a monthly stationkeeping maneuver is applied, the annual stationkeeping cost for the two LOP-G candidates would increases to around 25 m/s and 50 m/s respectively. It is noteworthy that the advantage of high-order TPA becomes apparent when the maneuver frequency is decreased, especially in the simulations related with the

Table 4
Optimal TPA parameters for the 1st candidate NRHO.

TPA Loop Scaling	Error Level	TPA Method	Annual $\|\|\Delta\mathbf{v}\|\|^{99}_{total}$ [m/s]	Δt_c [orbital period]	t_{TP1} [orbital period]	t_{TP2} [orbital period]	10^{ρ_1} [-]	10^{ρ_2} [-]
1	Low	H.O.	0.546	1.76E-05	0.653	1.561	1.59E-08	1.58E-03
		Lin	0.547	1.79E-05	0.926	1.789	5.18E-08	1.59E-03
	High	H.O.	3.446	1.76E-05	0.812	1.703	1.28E-09	3.96E-04
		Lin	3.436	1.76E-05	0.467	1.418	5.26E-08	3.97E-04
2	Low	H.O.	0.681	1.76E-05	1.168	3.168	2.35E-03	8.81E-03
		Lin	0.677	1.77E-05	1.905	3.655	1.21E-02	7.62E-03
	High	H.O.	4.590	2.27E-05	1.932	3.346	5.54E-10	2.21E-03
		Lin	4.740	1.76E-05	1.625	3.190	4.99E-04	1.98E-03
3	Low	H.O.	0.930	1.76E-05	1.699	4.472	3.41E-04	1.02E-02
		Lin	0.931	1.76E-05	2.657	4.944	4.78E-03	5.25E-03
	High	H.O.	7.589	1.76E-05	0.946	3.492	1.88E-02	8.80E-03
		Lin	7.922	1.76E-05	2.319	4.854	2.13E-10	5.05E-03
4	Low	H.O.	1.415	1.76E-05	2.633	6.310	1.01E-10	5.79E-03
		Lin	1.423	1.80E-05	2.825	6.745	5.05E-04	1.49E-02
	High	H.O.	12.338	1.76E-05	1.773	5.149	1.02E-10	3.14E-02
		Lin	13.469	1.77E-05	2.984	6.793	6.67E-02	2.14E-02
5	Low	H.O.	2.576	2.43E-05	4.710	8.498	4.31E-03	1.24E-03
		Lin	2.691	3.14E-05	3.750	8.405	1.87E-03	1.66E-02
	High	H.O.	25.249	1.77E-05	4.551	7.149	1.22E-02	5.49E-02
		Lin	25.360	1.76E-05	2.694	7.332	7.88E-01	8.82E-02

2nd candidate NRHO. According to the last two rows in Table 5, there is no optimal TPA parameters being found for the linear TPA, suggesting that it can no longer handle the high-level navigation errors with a TPA loop of five orbital periods. In comparison, the high-order TPA is still applicable in this case. In addition, among all the converged simulations in both tables, maneuvers are placed close to the apolune, which further demonstrates the importance of an early and timely maneuver in minimizing the influence from OD uncertainty. There is no remarkable regularity observed in the placement of TPs.

4.2. Stationkeeping analysis of quasi-satellite orbit

The QSO which is labeled as QSO-La and properly investigated in MMX mission (Baresi et al., 2021), is selected as a test case. Detailed orbital parameters of this candidate QSO are provided in Table 6, including the apoapsis/periapsis radius r_{apo}/r_{peri} and apoapsis/periapsis velocity v_{apo}/v_{peri}. Apart from being in remarkably close proximity to Phobos, the candidate QSO is also characterized by a symmetric elliptical shape and a much shorter orbital period in comparison with the candidate NRHOs. Naturally, such characteristics bring about several modifications in stationkeeping configurations.

The OD epoch is fixed at the apoapsis position for this QSO. Insertion and navigation errors are redefined with four different levels, where a 3σ velocity error of 1 cm/s is applied in all four levels and 3σ position errors vary from 200 m to 500 m. A 3σ maneuver execution error of 5% is assumed for each velocity component. A maneuver threshold of 1.5 mm/s is implemented and the maximum tolerance for position deviation Δd_{max} is reduced to 5 km. To satisfy a minimum maneuver frequency, one TPA loop is prolonged to 6 orbital periods, which is about 2 days, i.e., a more realistic interval between consecutive OD epoch (Baresi et al., 2021). The same GA setup and MC sample size as in the previous analysis are employed.

4.2.1. Simulation results

By means of the aforementioned stationkeeping configurations and optimization set-up, stochastic optimizations are launched with both TPA methods for the candidate QSO and optimal results are summarized in Table 7. It is observed that the linear TPA cannot find feasible solutions at the two highest error levels. Although it is applicable in the other two error levels, the annual maneuver costs are much higher than the corresponding costs of its high-order counterpart and even failed MC runs are spotted in the second error level. In comparison, the high-order TPA establishes its superiority in maneuver cost and uncertainty tolerance, which makes it a more reliable approach for maneuver calculation in this case. Moreover, it is confirmed that the optimal TPA parameters achieved by high-order TPA cannot be adopted by the linear TPA, since the distant downstream locations of 2nd TPs result in a low accuracy in the STM calculation, which further ends in the failures of the linear TPA.

4.3. Discussion

In both test cases, comparisons are made between the linear TPA and its high-order counterpart. It is undisputed that the results of linear TPA are sufficiently satisfactory in multiple stationkeeping cases. However, the linear TPA

Table 5
Optimal TPA parameters for the 2nd candidate NRHO.

TPA Loop Scaling	Error Level	TPA Method	Annual $\|\|\Delta\mathbf{v}\|\|^{99}_{total}$ [m/s]	Δt_c [orbital period]	t_{TP1} [orbital period]	t_{TP2} [orbital period]	10^{ρ_1} [-]	10^{ρ_2} [-]
1	Low	H.O.	0.715	1.59E-05	0.736	1.664	2.41E-03	9.10E-05
		Lin	0.732	2.78E-04	0.688	1.612	1.04E-03	9.72E-05
	High	H.O.	4.748	1.57E-05	0.618	1.377	1.52E-04	2.41E-04
		Lin	4.895	1.57E-05	0.741	1.312	1.29E-08	1.95E-03
2	Low	H.O.	1.044	1.57E-05	1.397	3.256	3.18E-05	2.96E-02
		Lin	1.055	1.57E-05	1.350	3.104	9.49E-05	9.41E-03
	High	H.O.	8.646	1.57E-05	1.991	3.006	1.63E-02	6.08E-03
3	Low	H.O.	1.954	1.57E-05	1.213	3.643	7.71E-10	1.13E-02
		Lin	2.066	1.57E-05	0.913	3.406	2.08E-09	1.12E-01
	High	H.O.	19.126	1.57E-05	2.612	3.418	6.86E-09	2.29E-02
		Lin	19.733	1.57E-05	2.531	5.032	1.45E-08	5.50E-02
4	Low	H.O.	4.546	1.60E-05	2.758	5.642	8.74E-08	6.83E-02
		Lin	4.724	1.57E-05	3.761	7.341	8.75E-10	9.09E-02
	High	H.O.	45.094	1.57E-05	1.576	3.700	1.09E-01	4.01E-01
		Lin	56.278	1.17E-01	2.740	6.306	1.13+00	5.77E-01
5	Low	H.O.	10.696	1.59E-05	2.175	5.369	1.86E-02	2.40E-01
		Lin	12.730	1.57E-05	3.931	8.273	1.00E-01	2.20E-01
	High	H.O.	197.252	1.64E-01	0.731	4.361	2.29+03	1.11+03
		Lin	N/A	N/A	N/A	N/A	N/A	N/A

Table 6
Parameters of the candidate QSO.

	$r_{apo} \times r_{peri}$ (km)	$v_{apo} \times v_{peri}$ (m/s)	Orbital Period (hour)	Stability Indices
QSO-La	48.84×30	8.68×15.31	5.76	$\nu_1 = -0.442$ $\nu_2 = 0.571$

Table 7
Optimal TPA parameters for QSO-La.

Error Level	TPA Method	Annual $\|\|\Delta\mathbf{v}\|\|^{99}_{total}$ [m/s]	Δt_c [orbital period]	t_{TP1} [orbital period]	t_{TP2} [orbital period]	10^{ρ_1} [-]	10^{ρ_2} [-]
200 m, 1 cm/s	H.O.	0.488	0.744	3.052	5.138	7.55E-04	3.04E-09
	Lin	1.344	1.015	1.814	4.384	3.12E-03	3.02E-04
300 m, 1 cm/s	H.O.	1.027	0.746	1.518	8.914	5.19E-03	1.20E-05
	Lin	5.892 (7 failures)	1.032	1.688	6.569	1.37E-02	1.78E-06
400 m, 1 cm/s	H.O.	4.935	0.919	1.774	7.828	2.17E-01	2.06E-01
	Lin	N/A	N/A	N/A	N/A	N/A	N/A
500 m, 1 cm/s	H.O.	16.608 (4 failures)	0.126	1.293	5.185	1.70+00	2.30E-09
	Lin	N/A	N/A	N/A	N/A	N/A	N/A

would underperform when handling an unstable periodic orbit, targeting a distant downstream TP, and dealing with operational constraints such as the time required between consecutive OD epochs. Under these scenarios, the key element of linear TPA, the linear approximation of state residuals based on STMs, fails to describe the dynamics accurately. To overcome such a deficiency, high-order TPA can be applied and meanwhile, bring a better tolerance to the navigation uncertainties.

Apart from the generality to be adopted for the maintenance of different periodic orbits, the test cases suggest a potential adoption of the TPA-based stationkeeping strategy for on-board spacecraft guidance. Once a set of optimal TPA parameters are determined, the high-order ODE expansions and maneuver map can be generated and stored. They can be rapidly evaluated at the predetermined stationkeeping epochs to acquire accurate orbit states and corrective maneuvers. This nonlinear stationkeeping framework can be further investigated for a future autonomous navigation system.

5. Conclusions

This paper proposed a nonlinear stationkeeping strategy based on Target Point Approach (TPA) for periodic orbits in the Circular Restricted Three-Body Problem. A stochastic optimization framework was developed in search of fuel-optimal and error-robust TPA parameters. A high-

order TPA method was proposed to realize a more accurate maneuver calculation. Orbital periodicity was leveraged to streamline the TPA-based stationkeeping strategy. Orbit determination epochs were chosen by means of a sensitivity analysis based on the convergence radius of a stroboscopic map. Monte Carlo simulations were efficiently embedded in the stationkeeping optimization by virtue of high-order ODE expansions. Stationkeeping analyses for both candidate Near Rectilinear Halo Orbits and Quasi-Satellite Orbits were executed to assess the performance of the proposed strategy. It was found that the high-order TPA method outperformed its linear counterpart in tackling high navigation uncertainty and handling unstable periodic orbits in fast dynamical environments.

Declaration of Competing Interest

The authors declare that they have no known competing financial interests or personal relationships that could have appeared to influence the work reported in this paper.

Acknowledgments

Xiaoyu Fu is funded by Vice-Chancellor's Studentship of the University of Surrey. The authors acknowledge the University of Surrey for providing access to their High Performance Cluster 'Eureka' resources that have contributed to the research results reported within this paper.

References

Armellin, R., Di Lizia, P., Berz, M., et al., 2010a. Computing the critical points of the distance function between two Keplerian orbits via rigorous global optimization. Celestial Mech. Dyn. Astron. 107 (3), 377–395. https://doi.org/10.1007/s10569-010-9281-7.

Armellin, R., Di Lizia, P., Topputo, F., et al., 2010b. Gravity assist space pruning based on differential algebra. Celestial Mech. Dyn. Astron. 106 (1), 1–24. https://doi.org/10.1007/s10569-009-9235-0.

Armellin, R., San-Juan, J.F., Lara, M., 2015. End-of-life disposal of high elliptical orbit missions: The case of INTEGRAL. Adv. Space Res. 56 (3), 479–493. https://doi.org/10.1016/j.asr.2015.03.020.

Baresi, N., Dei Tos, D.A., Ikeda, H., et al., 2021. Trajectory design and maintenance of the Martian moons eXploration mission around Phobos. J. Guidance, Control, Dyn. 44 (5), 996–1007. https://doi.org/10.2514/1.G005041.

Berz, M., 1999. Modern Map Methods in Particle Beam Physics. Academic Press, Cambridge.

Crusan, J.C., Smith, R.M., Craig, D.A. et al., 2018. Deep space gateway concept: Extending human presence into cislunar space. In: IEEE Aerospace Conference, pp. 1–10. https://doi.org/10.1109/AERO.2018.8396541.

Davis, D., Bhatt, S., Howell, K. et al., 2017. Orbit maintenance and navigation of human spacecraft at cislunar near rectilinear halo orbits. In: 27th AAS/AIAA Space Flight Mechanics Meeting. AAS 17-269.

Dei Tos, D.A., Baresi, N., 2020. Genetic optimization for the orbit maintenance of libration point orbits with applications to EQUULEUS and LUMIO. In: AIAA Scitech 2020 Forum, p. 0466. https://doi.org/10.2514/6.2020-0466.

Dei Tos, D.A., Yamamoto, T., Ozaki, N. et al., 2020. Operations-driven low-thrust trajectory optimization with applications to DESTINY+. In: AIAA SciTech 2020 Forum, p. 2182. https://doi.org/10.2514/6.2020-2182.

Fu, X., Baresi, N., Armellin, R., 2020. A High-order Target Point Approach to the Stationkeeping of Near Rectilinear Halo Orbits. In: 71th International Astronautical Congress, CyberSpace Edition. IAC-20-C.1.6.3.

Ghorbani, M., Assadian, N., 2013. Optimal station-keeping near Earth-Moon collinear libration points using continuous and impulsive maneuvers. Adv. Space Res. 52 (12), 2067–2079. https://doi.org/10.1016/j.asr.2013.09.021.

Gómez, G., Howell, K., Masdemont, J., et al., 1998. Station-keeping strategies for translunar libration point orbits. Adv. Astronaut. Sci. 99 (2), 949–967.

Gurfil, P., Meltzer, D., 2006. Stationkeeping on unstable orbits: generalization to the elliptic restricted three-body problem. J. Astronaut. Sci. 54 (1), 29–51. https://doi.org/10.1007/BF03256475.

Guzzetti, D., Zimovan, E.M., Howell, K.C. et al., 2017. Stationkeeping analysis for spacecraft in lunar near rectilinear halo orbits. In: 27th AAS/AIAA Space Flight Mechanics Meeting. AAS 17-395.

Hénon, M., 1969. Numerical exploration of the restricted problem. Astron. Astrophys. 1, 223–238.

Howell, K.C., Keeter, T.M., 1995. Station-keeping strategies for libration point orbit - Target Point and Floquet Mode approaches. Spaceflight Mechanics 1995, pp. 1377–1396.

Howell, K.C., Pernicka, H.J., 1993. Station-keeping method for libration point trajectories. J. Guidance, Control, Dyn. 16 (1), 151–159. https://doi.org/10.2514/3.11440.

Jenson, E.L., Scheeres, D.J., 2021a. Multi-Objective Optimization of Covariance and Energy for Asteroid Transfers. J. Guidance, Control, Dyn. 44 (7), 1253–1265. https://doi.org/10.2514/1.G005609.

Jenson, E.L., Scheeres, D.J., 2021b. Semianalytical Measures of Nonlinearity Based on Tensor Eigenpairs. In: AAS/AIAA Astrodynamics Specialist Conference.

Kulkarni, J.E., Campbell, M.E., Dullerud, G.E., 2006. Stabilization of Spacecraft Flight in Halo Orbits: An H_∞Approach. IEEE Trans. Control Syst. Technol. 14 (3), 572–578. https://doi.org/10.1109/TCST.2006.872517.

Morselli, A., Armellin, R., Di Lizia, P., et al., 2014. A high order method for orbital conjunctions analysis: sensitivity to initial uncertainties. Adv. Space Res. 53 (3), 490–508. https://doi.org/10.1016/j.asr.2013.11.038.

Muralidharan, V., Howell, K.C., 2020. Stationkeeping in Earth-Moon Near Rectilinear Halo Orbits. In: AAS/AIAA Astrodynamics Specialist Conference. AAS 20-642.

Oberst, J., Wickhusen, K., Willner, K., et al., 2018. DePhine–The Deimos and Phobos Interior Explorer. Adv. Space Res. 62 (8), 2220–2238. https://doi.org/10.1016/j.asr.2017.12.028.

Oguri, K., Oshima, K., Campagnola, S., et al., 2020. EQUULEUS Trajectory design. J. Astronaut. Sci. 67 (3), 950–976. https://doi.org/10.1007/s40295-019-00206-y.

Ren, Y., Shan, J., 2015. Reliability-based soft landing trajectory optimization near asteroid with uncertain gravitational field. J. Guidance, Control, Dyn. 38 (9), 1810–1820. https://doi.org/10.2514/1.G000903.

Ross, I.M., Proulx, R., Karpenko, M., 2014. Unscented optimal control for orbital and proximity operations in an uncertain environment: A new Zermelo problem. In: AAS/AIAA Astrodynamics Specialist Conference. https://doi.org/10.2514/6.2014-4423.

Scheeres, D.J., Hsiao, F.-Y., Vinh, N.X., 2003. Stabilizing motion relative to an unstable orbit: applications to spacecraft formation flight. J. Guidance, Control, Dyn. 26 (1), 62–73. https://doi.org/10.2514/2.5015.

Shirobokov, M., Trofimov, S., Ovchinnikov, M., 2017. Survey of station-keeping techniques for libration point orbits. J. Guidance, Control, Dyn. 40 (5), 1085–1105. https://doi.org/10.2514/1.G001850.

Williams, J., Lee, D.E., Whitley, R.J. et al., 2017. Targeting cislunar near rectilinear halo orbits for human space exploration. In: 27th AAS/AIAA Space Flight Mechanics Meeting.

Wittig, A., Di Lizia, P., Armellin, R., et al., 2015. Propagation of large uncertainty sets in orbital dynamics by automatic domain splitting. Celestial Mech. Dyn. Astron. 122 (3), 239–261. https://doi.org/10.1007/s10569-015-9618-3.

Xu, M., Xu, S., 2009a. Exploration of distant retrograde orbits around Moon. Acta Astronaut. 65 (5–6), 853–860. https://doi.org/10.1016/j.actaastro.2009.03.026.

Xu, M., Xu, S., 2009b. Structure-preserving stabilization for hamiltonian system and its applications in solar sail. J. Guidance, Control, Dyn. 32 (3), 997–1004. https://doi.org/10.2514/1.34757.